Pressure-induced bcc-rhombohedral phase transition in vanadium metal

M. G. Stevenson,[1] E. J. Pace,[1] C. V. Storm,[1] S. E. Finnegan [orcid],[1] G. Garbarino,[2] C. W. Wilson,[3] D. McGonegle,[3] S. G. Macleod [orcid],[3,1] and M. I. McMahon [orcid][1]

[1]*SUPA, School of Physics and Astronomy, and Centre for Science at Extreme Conditions, The University of Edinburgh, Mayfield Road, Edinburgh EH9 3JZ, United Kingdom*
[2]*European Synchrotron Radiation Facility, Grenoble 38043, France*
[3]*AWE, Aldermaston, Reading RG7 4PR, United Kingdom*

Vanadium is reported to undergo a pressure-induced bcc-rhombohedral phase transition at 30–70 GPa, with a transition pressure that is sensitive to the hydrostaticity of the sample environment. However, the experimental evidence for the structure of the high-pressure phase being rhombohedral is surprisingly weak. We have restudied vanadium under pressure to 154 GPa using both polycrystalline and single-crystal samples, and a variety of different pressure transmitting media (PTM). We find that only when using single-crystal samples does one observe a rhombohedral high-pressure phase; the high-pressure diffraction profiles from the polycrystalline samples do not fit a rhombohedral lattice, irrespective of the PTM used. The single-crystal samples reveal two rhombohedral phases, with a continuous transition between them, and distortions from cubic symmetry are much smaller than previously calculated.

I. INTRODUCTION

The structural behavior of vanadium (V) on compression is unique amongst the elements. Initial x-ray diffraction studies by Takemura using He and methanol:ethanol pressure transmitting media (PTM) reported that V remained in the body centered cubic (bcc) phase until 154 GPa, although a published diffraction profile at 154 GPa suggests that the first diffraction peak had become highly asymmetric, or even a doublet, at this pressure [1]. A subsequent diffraction study by Nakamoto *et al.* to 224 GPa, using a He PTM at lower pressures and no PTM at higher pressures, also reported no phase transition, and the peak asymmetry shown (but not commented on) by Takemura was not evident [2].

However, concurrent lattice dynamics calculations, aimed at understanding the anomaly in the superconducting temperature of V near 120 GPa [3], found that the transverse acoustic phonon mode shows a dramatic softening under pressure and becomes imaginary at pressures above ∼130 GPa, suggesting the possibility of a structural phase transition [4]. Subsequent calculations of the trigonal shear elastic constant (C_{44}) of V showed it became negative just below 200 GPa, suggesting that bcc-V is mechanically unstable under trigonal shear [5]. Inspired by these calculations, Ding *et al.* restudied powdered V with no PTM to 155 GPa using x-ray diffraction and reported a phase transition from bcc to a rhombohedral phase at 63 GPa [6] with no volume discontinuity. The same transition was seen at the slightly higher pressure of 69 GPa when a He PTM was used. Ding *et al.* reported that the phase transition could be associated with the softening of the C_{44} trigonal elasticity tensor originating from the combination of Fermi surface nesting, band Jahn-Teller distortion, and a electronic

topological transition. A subsequent x-ray diffraction study by Jenei *et al.* [7] confirmed the bcc to rhombohedral phase transition, which they located at 65 GPa using a He PTM, at 61.5 GPa using a Ne PTM, and at only 30 GPa when using no PTM. They also observed no volume change at the transition.

Motivated by the measurements of Ding *et al.* [6], Lee *et al.* performed first-principles electronic-structure calculations which confirmed the existence of the rhombohedral phase, (rhomb1) which they calculated to be the ground state at zero temperature at 84 GPa. They also predicted two further phase transitions not seen by Ding *et al.*—a first-order transition to a second rhombohedral structure (rhomb2) at 120 GPa, followed by a transition back to the bcc phase at 280 GPa [8]. The same transition sequence—bcc→rhomb1→ rhomb2 → bcc—was also seen in the computational study of Luo *et al.* [9], who reported the three transitions to occur at 62 GPa, 130 GPa, and 250 GPa, and in the computational studies of Qiu and Marcus [10], Verma and Modak [11], and Wang *et al.* [12]. In each study, rhomb1 was reported to have a rhombohedral angle of $\alpha \sim 110.5°$, while rhomb2 has $\alpha \sim 108.5°$.

This unusual behavior has an impact on the pressure dependence of V's strength. Diamond anvil cell (DAC) measurements to 90 GPa have shown that the shear strength of V first increases with pressure up to around 40–50 GPa, that is before the transition to the rhombohedral phase, and then decreases on further compression [13]. Furthermore, finite-temperature computational studies by Yu *et al.* have predicted that the strength of V will increase with increasing temperature due to unusual hardening of the C_{44} shear modulus with temperature [14].
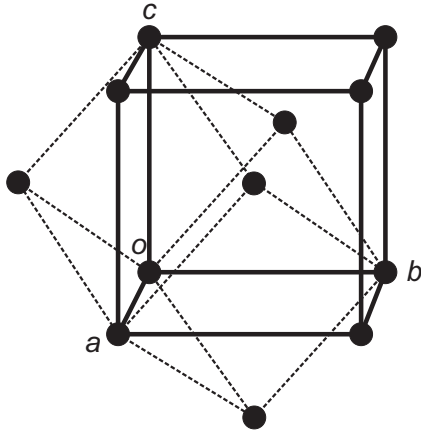
FIG. 1. The body-centred unit cell of vanadium (solid lines) and the corresponding primitive rhombohedral cell (dashed lines). A cubic body-centred cell with lattice parameter a_c can be considered a rhombohedral cell with $a_r = a_c \frac{1}{2}\sqrt{3}$ and $\alpha = 109.47°$ (rhombohedral axes) or a triple hexagonal cell with $a_h = \sqrt{2}a_c$, $c_h = a_c \frac{1}{2}\sqrt{3}$, and $c_h/a_h = \sqrt{3/8}$ (hexagonal axes).
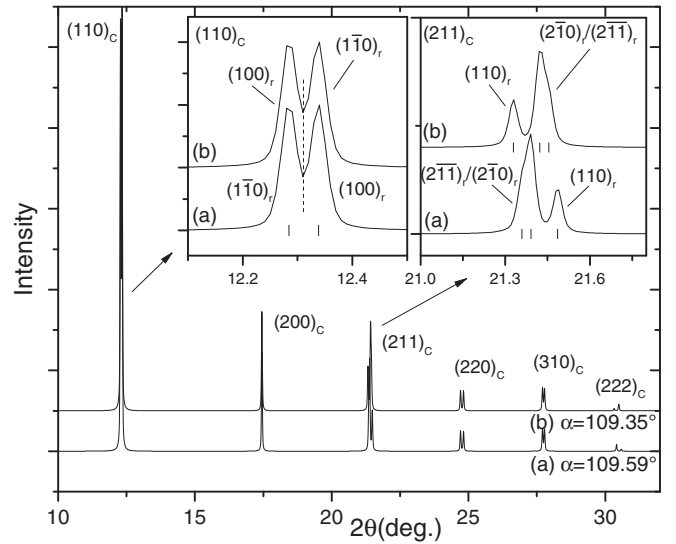

FIG. 2. Calculated diffraction patterns for two rhombohedral V structures with (a) $a_r = 2.4284$ Å, $\alpha = 109.59°$ and (b) $a_r = 2.4213$ Å, $\alpha = 109.35°$. Both structures have the same density. The peaks in the main part of the figure are indexed with their bcc Miller indices. The left-hand inset illustrates how the change in α from $109.47°$ results in the $(110)_c$ peak splitting evenly about its position in a bcc phase with the same density, shown by the vertical dashed line. The right-hand inset illustrates how the $(211)_c$ peak splits into a triplet in the rhombohedral phase, the peaks of which are in different positions in the two different structures. Whether α is > or <$109.47°$ can therefore be determined from the positions and relative intensities of the peaks that form this triplet in the rhombohedral phase.

Finally, the high-temperature behavior of V, and its melting curve, have been the subject of two recent studies by Errandonea *et al.* [15] and Zhang *et al.* [16]. Using a DAC, Errandonea *et al.* mapped the bcc-rhombohedral transition at elevated temperatures, and showed that only the bcc phase is observed above ~1800 K at 60 and 120 GPa [15]. The tentative bcc-rhombohedral phase boundary suggested that the Hugoniot would pass through the rhombohedral phase between 60 and 110 GPa.

Zhang *et al.* used both static and dynamic compression techniques, as well as *ab initio* molecular dynamics and DFT calculations, to investigate V to ~256 GPa and ~6200 K [16]. They reported the bcc-rhombohedral transition to occur at ~50 GPa at room temperature, and also mapped out the bcc-rhombohedral transition at elevated temperatures, finding only the bcc phase above 1500-1600 K between 52 and 100 GPa.

There is thus a considerable body of both experimental and computational work on V that reports a bcc-rhombohedral transition between 30 and 70 GPa. However, reanalysis of the published diffraction data that provide the key experimental evidence for the transition (as described below in Sec. III) shows that the data do not fit the claimed rhombohedral structure. We have therefore made a comprehensive study of polycrystalline and single-crystal V to 154 GPa, using a range of PTMs, to investigate its behavior. We find unusual behavior in the polycrystalline samples from remarkably low pressures, and confirm that the diffraction patterns from polycrystalline samples are not well fitted by either cubic or rhombohedral structures. Much better fits are obtained to data obtained from single crystals, which reveal previously unobserved behavior above 40 GPa.

II. THE BCC-RHOMBOHEDRAL TRANSITION

The bcc structure with the lattice parameter a_c, shown in Fig. 1, can also be described using a primitive rhombohedral structure with $a_r = (\sqrt{3}/2)a_c$ and $\alpha = 109.47°$ (rhombo-

hedral axes) or a triple hexagonal cell with $a_h = \sqrt{2}a_c$, $c_h = (\sqrt{3}/2)a_c$, $c_h/a_h = \sqrt{3/8}$ (hexagonal axes) [17]. The high-pressure rhombohedral phase in V has typically been described using the rhombohedral axes, and thus the distortion of the unit cell from cubic symmetry is described by changes in the α angle from the "cubic" value of $109.47°$. For example, Ding *et al.* reported that $\alpha = 109.65(5)°$ at 90 GPa, increasing to $109.82(5)°$ at 155 GPa [6], while Jenei *et al.* refined a value of $109.61(2)°$ at 30 GPa [7]. The second rhombohedral phase of V calculated to exist above 120 GPa [8–11], but not yet observed experimentally, is characterized by having an α angle *smaller* than the cubic value of $109.47°$.

The reduction in symmetry at the cubic-rhombohedral transition results in a splitting of some (but not all) of the bcc diffraction peaks, as shown in Fig. 2. Specifically, the $(110)_c$, $(211)_c$, $(220)_c$, $(310)_c$, and $(222)_c$ peaks from the bcc phase all split into two or more peaks, as follows, with the degree of splitting dependant on the value of α, while the $(200)_c$ remains unsplit.

$$(110)_c \rightarrow (1\bar{1}0)_r + (100)_r,$$
$$(200)_c \rightarrow (1\bar{1}1)_r,$$
$$(211)_c \rightarrow (2\bar{1}\bar{1})_r + (20\bar{1})_r + (110)_r,$$
$$(220)_c \rightarrow (2\bar{2}0)_r + (200)_r,$$
$$(310)_c \rightarrow (21\bar{1})_r + (21\bar{2})_r,$$
$$(222)_c \rightarrow (3\bar{1}\bar{1})_r + (111)_r.$$

The value of α can thus be obtained from the splitting of the cubic $(110)_c$, $(211)_c$, etc. diffraction peaks, and, *vice versa*, the single parameter α determines the degree of splitting of the diffraction peaks.

While the description of the rhombohedral phase using the primitive unit cell with $\alpha \sim 109.47°$ has been used in all previous diffraction studies of V, the required change in the indexing of the diffraction peaks at the cubic-rhombohedral transition makes a direct comparison with the same peaks in the bcc structure difficult. In the single-crystal study described later in Sec. V C, it proved useful to describe the rhombohedral phase using a nonprimitive bcc-like setting where $a_{r'} \sim a_c$ and $\alpha' \sim 90°$, such that the indexing of individual Bragg peaks remained unchanged on passing through the cubic-rhombohedral transition. However, for consistency and comparison, the lattice parameters of this nonprimitive bcc-like setting were converted back to those from the equivalent primitive unit cell.

At this point, it is also instructive to determine whether one can distinguish whether α is greater or less than 109.47° from the powder diffraction pattern alone (or, equivalently, whether α' is greater or less than 90° in the body-centred rhombohedral setting, or whether c_h/a_h is greater or less than $\sqrt{3/8}$ in the triple-hexagonal setting). Distinguishing whether α is greater or less than 109.47° is essential in order to distinguish the rhomb1 and rhomb2 structures.

Figure 2 shows two calculated diffraction patterns with (a) $a_r = 2.4284$Å, $\alpha = 109.59°$ and (b) $a_r = 2.4213$ Å, $\alpha = 109.35°$. The densities of the two structures are the same. It can be seen that the splitting of the cubic $(110)_c$, $(220)_c$, and $(310)_c$ peaks is identical in the two diffraction patterns (although the rhombohedral indices of the left- and right-hand peaks in each doublet are different, as illustrated in the left-hand inset), and the unsplit $(200)_c$ peak is in the same position in each profile. None of these peaks can therefore be used in a powder-diffraction profile to determine whether α is greater or smaller than 109.47°. However, the bcc $(211)_c$ peak splits into a triplet (the $(110)_r$, $(20\bar{1})_r$ and $(2\bar{1}1)_r$) at the cubic-rhombohedral transition, and the positions of the three peaks are different in the two structures, as highlighted in the right-hand inset of Fig. 2. The same is also true of the higher-angle $(222)_c$ peak (not shown enlarged), and so the splitting of the $(211)_c$ and the $(222)_c$ peaks (that is, peaks with $h, k, l \neq 0$) *can* be used to distinguish the two structures. The arrangement of the peaks in the $(211)_c$ triplet reveals that two of them are close together, and that the combined, more intense peak is at lower angles when $\alpha > 109.47°$ and at higher angles when $\alpha < 109.47°$. Even if the positions of the three individual peaks that make up the $(211)_c$ triplet cannot be discerned in a diffraction profile, therefore, the intensity distribution in the triplet might still be used to distinguish the two structures.

Finally, the left-hand inset to Fig. 2 shows an enlarged view of the $(110)_c$ doublet, along with the calculated position of the unsplit peak in the cubic phase, assuming a lattice parameter of $a_c = 2.8$ Å and hence the same density as the two rhombohedral structures. It can be seen that the peaks that form the doublet split evenly, in d spacing, about the dashed line.

Therefore the d-spacing ratios of the $(1\bar{1}0)_r$ and $(100)_r$ doublet with respect to the $(1\bar{1}1)_r$ singlet diverge from the
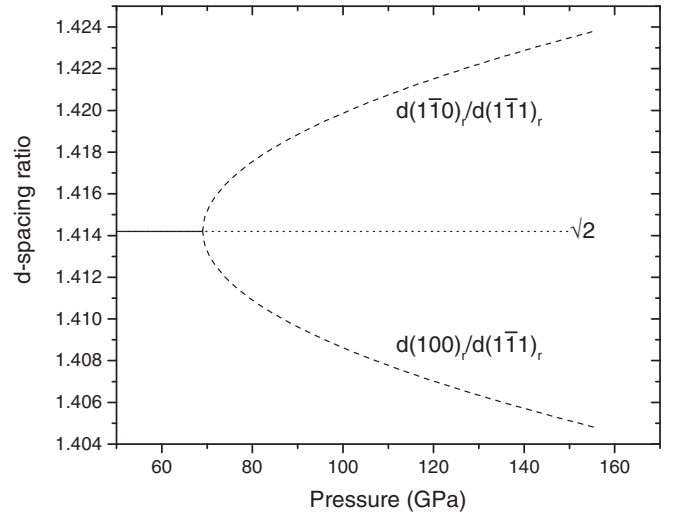

FIG. 3. The d-spacing ratios of the $(1\bar{1}0)_r/(1\bar{1}1)_r$ and $(100)_r/(1\bar{1}1)_r$ reflections (primitive rhombohedral indexing), as *calculated* from the rhombohedral fits to the nonhydrostatic data reported by Ding *et al.* [6]. At the transition at 69 GPa, the ratios split equally about the value of $\sqrt{2}$, with the degree of splitting depending only on the rhombohedral angle. If the same ratios derived from the *observed* peak positions do not exhibit a similar symmetric splitting, then the positions of the three peaks are inconsistent with a rhombohedral lattice.

value of 1.414 ($\sqrt{2}$), the ratio of the equivalent peaks in the cubic structure ($(110)_c$ and $(200)_c$), with one being greater than $\sqrt{2}$ and the other less than $\sqrt{2}$. This behavior is illustrated in Fig. 3 which shows the d-spacing ratios of these reflections, as calculated from the structural parameters obtained by Ding *et al.* [6] from their nonhydrostatic data. As we plot the ratios of the peak positions, the splitting about $\sqrt{2}$ depends only on the rhombohedral angle α, and not on the dimension of the unit cell a_r. If this symmetric splitting about $\sqrt{2}$ is not reproduced using the observed d spacings of these three peaks in the diffraction data then they cannot be fitted simultaneously with a rhombohedral lattice.

III. FITS OF PREVIOUS DATA

The first diffraction study of V to pressures where the rhombohedral phase might have been seen was made by Takemura who reported no phase transition or equation of state (EoS) anomaly up to 154 GPa [1]. However, the diffraction pattern obtained at 154 GPa shows the $(110)_c$ peak to be asymmetric, and perhaps better described as a doublet, while the $(200)_c$ peak remained a sharp singlet [1]. Unfortunately, the limited angular range of the data prevented any analysis of the $(211)_c$ peak. The data of Nakamoto *et al.* [2] show no evidence of a cubic-rhombohedral transition up to 51 GPa, and while the authors reported no transition up to 224 GPa, the overlap of peaks from the Re gasket with the $(110)_c$ peak from the V at these pressures makes it difficult to determine whether the peak splits or not.

The diffraction study of Ding *et al.* [6] reported the onset of the transition to the rhombohedral phase at 63 GPa in a quasihydrostatic sample and 69 GPa in a nonhydrostatic

sample. Splittings of the Debye-Scherrer rings consistent with a bcc-rhombohedral transition were observed in both the integrated profiles, and, at higher pressures, in the 2D diffraction images themselves. At 90 and 155 GPa, the rhombohedral angles was reported to be $\alpha = 109.65°$ and $109.82°$, respectively. However, the intensity distribution in the $(211)_c$ triplet at these two pressures suggests, rather, that the rhombohedral angle is $<109.47°$ at 90 GPa, but $>109.47°$ at 155 GPa. Ding *et al.* showed no Rietveld fits to their data, but only illustrated how the $(110)_c$ and $(211)_c$ peaks of the bcc phase can be resolved into a doublet and triplet, respectively, in the rhombohedral phase at 155 GPa. However, the positions of the peaks they show are both (i) inconsistent with a rhombohedral lattice (their relative positions are wrong) and (ii) inconsistent with the lattice parameters they report at this pressure.

Although Jenei *et al.* [7] also saw a clear splitting of the $(110)_c$ peak in the 2D diffraction images at 82 GPa, they showed a Rietveld refinement of the rhombohedral phase only immediately above the transition at 30 GPa, where $a_r = 2.510(1)$Å and $\alpha = 109.61°$. However, as in the lower-pressure data of Ding *et al.* [6], the intensity distribution of the $(211)_c$ peak is strongest at higher angles, suggesting that a fit with $\alpha < 109.47°$ would give a better fit to their data.

Subsequent diffraction studies of V, such as the radial diffraction study of Xiong and Liu [18], also reported the bcc-rhombohedral transition at $\sim$30 GPa, as determined by the broadening and splitting of the $(110)_c$ and $(211)_c$ diffraction peaks, but showed no Rietveld fits. They reported a rhombohedral angle of $\alpha = 109.61°$ at 45 GPa, but the intensity distribution in the diffraction profiles suggest that an α angle of $<109.47°$ would give an equally good fit.

The high-temperature behavior of V, and its melting curve, have been the subject of two recent studies by Errandonea *et al.* [15] and Zhang *et al.* [16]. In the first of these, Errandonea *et al.* [15] showed a Rietveld fit to a profile from the rhombohedral phase at 64 GPa at 300 K, by far the highest pressure at which a such a fit has been published. The quoted lattice parameters at this pressure are $a_r = 2.431(1)$ Å and $\alpha = 109.47(5)°$, but the α angle is then that of a cubic cell, and thus cannot account for the split peak positions shown beneath the Rietveld fit. The correct lattice parameters from this fit are $a_r = 2.4268$ Å and $\alpha = 109.33°$ [19], and this is thus the first and only diffraction study to date where α has been determined as $<109.47°$, although, as described above, previous diffraction data are suggestive of α being less that $109.47°$ at both 30 GPa [7] and 90 GPa [6].

Zhang *et al.* utilized laser-heated x-ray diffraction techniques to study both phase transitions and melting in V to $\sim$100 GPa and $\sim$4400 K [16]. While they show diffraction patterns both on compression at 300 K, and as a function of temperature at 52 GPa, and report lattice parameters for both the bcc and rhombohedral phases, the tickmarks shown beneath the rhombohedral profiles at 52 GPa are not consistent with those lattice parameters. Indeed, the spacing of the peaks in the triplet that forms from the $(211)_c$ peak (as illustrated in Fig. 2) are not consistent with a rhombohedral lattice. It is therefore unclear as to how the given lattice parameters were obtained, or what constraints, if any, were used in the peak fitting shown.

Despite the numerous high-pressure diffraction studies of V, there remain a number of outstanding questions as to its structural behavior. Is there a cubic $\rightarrow$ rhombohedral transition in V at 30–60 GPa, and does this rhombohedral phase have $\alpha < $ or $> 109.47°$? Is there a second, rhomb1$\rightarrow$ rhomb2 structural transition at $\sim$120 GPa, involving a discontinuous change in α from $\sim$110.5° to $\sim$108.5°? And, finally, is there a re-entrant transition to the bcc phase at $\sim$250 GPa? To try and address these questions, and to address some of the issues, we have made a series of x-ray diffraction studies of V to 154 GPa using both powder and single-crystal samples in different pressure transmitting media.

IV. EXPERIMENT

The x-ray diffraction studies were conducted using synchrotron radiation on polycrystalline powders (Aldrich) of V, as well as [001]-oriented single crystals grown on a Mo single-crystal substrate. Angle-dispersive powder x-ray diffraction data were collected on the I15 beamline at the Diamond Light Source (DLS), beamline ID15B at the European Synchrotron Radiation Facility (ESRF), and on beamline P02.2 at the PETRA-III synchrotron. The single-crystal data were collected at PETRA-III. The exact x-ray wavelengths used in each data collection, and the sample-detector distances and detector tilts, were determined precisely at the start of each beam time using standard diffraction calibrants (CeO$_2$, LaB$_6$ and Si), and were typically $\sim$0.41 Å (DLS, ESRF, PETRA-III) or $\sim$0.29 (PETRA-III). Typical beam sizes were 20 μm (DLS), 10 μm (ESRF and PETRA-III), or 0.85 μm (PETRA-III).

The samples were loaded into a number of different DACs equipped with flat and beveled diamond anvils, depending on the upper pressure required, and tungsten or rhenium gaskets. Samples were loaded without a PTM and with mineral oil or He as a PTM. A small ruby sphere was loaded into the He-containing DAC as a pressure calibrant, while the cells with no PTM contained a small amount of Pt powder as a pressure calibrant [20]. The single crystal of V was mounted on a single-crystal Mo substrate, which acted as the pressure calibrant [20].

The 2D diffraction images data were collected on area detectors placed $\sim$350 mm from the sample and integrated into standard 1D diffraction profiles using DIOPTAS [21]. The diffraction profiles were then analysed using Rietveld or Le Bail profile-fitting techniques [22], or by fitting to the positions of individual Bragg peaks [23].

V. EXPERIMENTAL RESULTS

A number of different experiments were performed at three synchrotrons over a three-year period, and in the following discussion, we group these together under three sub-headings: nonhydrostatic compression of V powder; quasihydrostatic compression of V powder; and, finally, quasihydrostatic compression of V single crystals. The highest pressure reached in each case was 139, 154, and 118 GPa, respectively. These sub-headings enable us both to compare our results with those obtained from previous studies under similarly described experimental conditions, and also to highlight the similarities
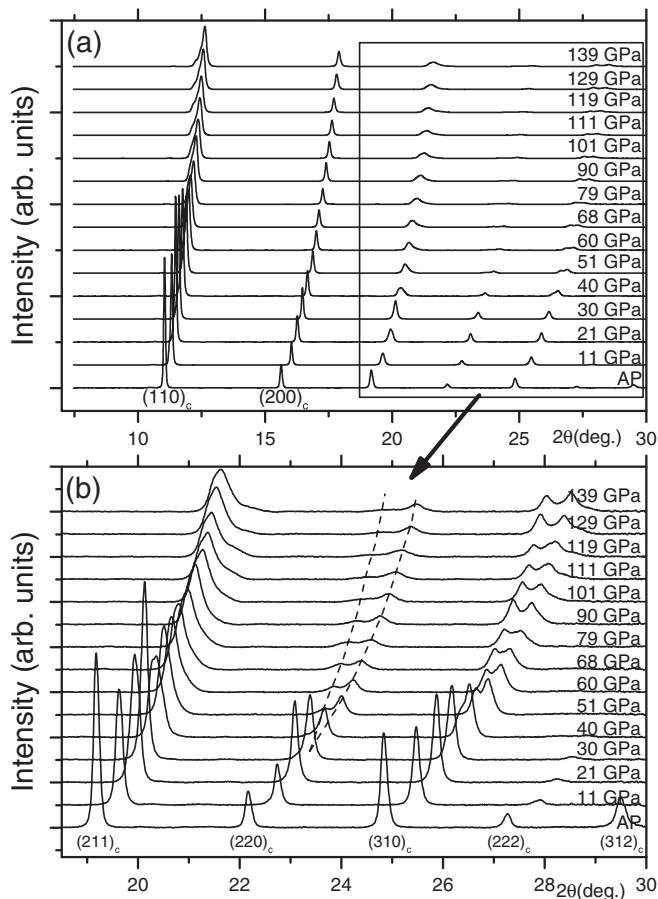
FIG. 4. (a) Diffraction profiles obtained from V compressed without a PTM up to 139 GPa. The incident x-ray wavelength was 0.4119 Å. The peaks in the ambient pressure (AP) profile are indexed using their bcc indices. (b) Enlarged view of the high-angled region of the profiles. The splitting of the bcc peaks above 30 GPa is clear, and is highlighted with dashed lines for the (220) peak.

and differences observed in the behavior of the V as a result of the differences in experimental conditions. For clarity, we do not show all of the data collected under each heading, but typically only data from the samples that reached the highest pressure in each case. However, the data collected from the lower-pressure samples were completely consistent with the data shown in all cases.

A. Nonhydrostatic compression of V powder

This series of experiments reproduces the nonhydrostatic diffraction studies of Takemura [1], Nakamoto *et al.* [2], Ding *et al.* [6], and Jenei *et al.* [7]. In preparing the samples we completely filled the gasket hole with powdered V, along with a few grains of Pt powder as a pressure marker. The pressure was increased in 2–5 GPa increments from ambient pressure to 139 GPa. At each pressure a diffraction image was obtained both with peaks from the Pt, and without. A selection of the Pt-free diffraction profiles obtained in ∼10 GPa increments is shown in Fig. 4.

It is clear that the bcc peaks split above 30 GPa—indeed the first evidence of splitting is seen at 36 GPa, some 6 GPa
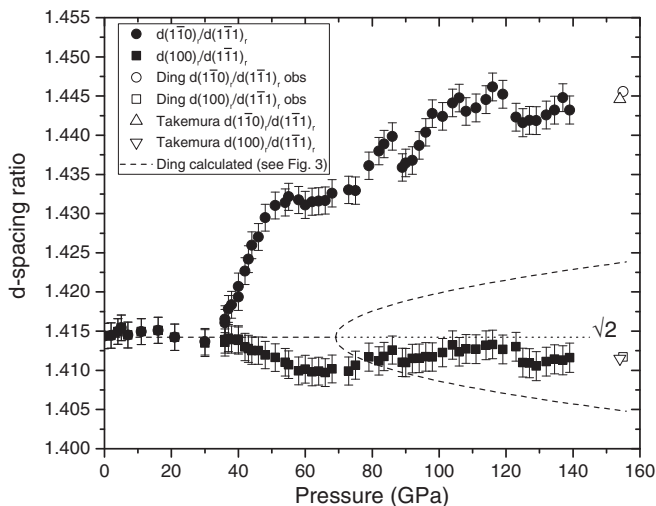

FIG. 5. The pressure dependence of d-spacing ratio of the $(1\bar{1}0)_r$ and $(100)_r$ reflections relative to the $(1\bar{1}1)_r$ reflection for V compressed without a PTM. In the bcc phase the ratio is $\sqrt{2}$, while in the rhombohedral phase the two ratios change such that one is $> \sqrt{2}$ and the other is $< \sqrt{2}$, but their average remains $\sqrt{2}$, as shown by the dashed line. The deviation from this behavior means that a rhombohedral lattice cannot fit the $(1\bar{1}0)_r$, $(100)_r$ and $(1\bar{1}1)_r$ reflections simultaneously. Also shown are the values calculated from the diffraction profile shown by Ding *et al.* at 155 GPa [6] and the diffraction profile of Takemura at 154 GPa [1]. The agreement of these two previous studies with the current data is excellent.

above the value reported by Jenei *et al.* in a nonhydrostatic environment. The appearance of the diffraction profiles above 36 GPa is very similar to that reported previously [6,7], with the $(200)_c$ peak remaining a singlet, but with the others splitting into doublets or triplets. However, attempts to fit the diffraction profiles above 36 GPa with the rhombohedral structure were unsuccessful, as a rhombohedral lattice simply does not give a good fit to the observed peak positions. One way to demonstrate this, as described previously in Sec. III, is shown in Fig. 5, which plots the ratio of the d spacings of the two reflections that form from the $(110)_c$ bcc peak (the $(1\bar{1}0)_r$ and $(100)_r$) to that of the $(200)_c$ bcc peak (the $(1\bar{1}1)_r$). In the bcc structure, the ratio is exactly $\sqrt{2}$, and in the rhombohedral phase the ratios should split equally about this value, as illustrated in Fig. 2, such that the average ratio remains $\sqrt{2}$. From Fig. 5, it is clear that this is NOT what happens and explains why a rhombohedral lattice does not fit the observed peak positions. The d-spacing ratios obtained from the diffraction profiles shown by Takemura at 154 GPa [1] and Ding *et al.* at 155 GPa [6] are in excellent agreement with those determined here, and show exactly the same effect, as illustrated in Fig. 5. In neither case, therefore, are the diffraction patterns consistent with a rhombohedral lattice.

The degree of misfitting of the diffraction profiles to a rhombohedral lattice is illustrated directly in Fig. 6, which shows a two-phase Rietveld fit to the profile obtained at 61 GPa. This profile contains peaks from the Pt calibrant, the positions of which are well fitted right across the profile. Therefore misfits due to calibration errors, etc. can be excluded as the reason for the poor fit to the rhombohedral
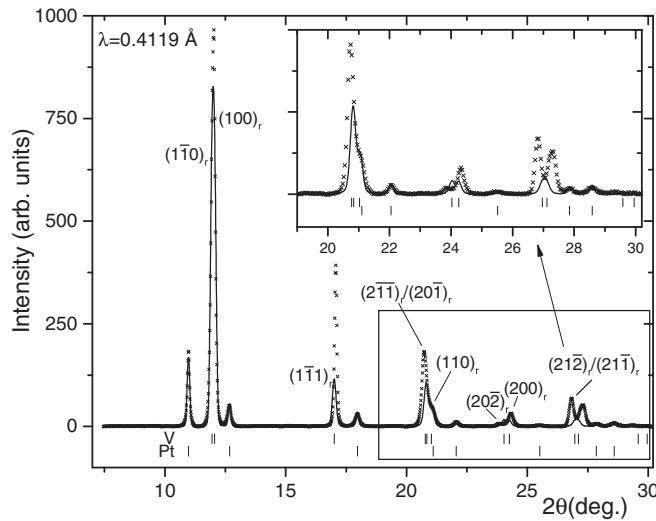
FIG. 6. A two-phase Rietveld profile fit to the diffraction profile from V and the Pt pressure marker compressed without a PTM at 61 GPa, showing the observed (crosses) and calculated (line) diffraction profiles. The calculated reflection positions for both the V and Pt are shown beneath the profiles. The positions of all of the Pt peaks are predicted precisely by the lattice parameter of $a = 3.729(1)$ Å. In contrast, the peak positions of the V are clearly *not* correctly predicted by the best-fitting rhombohedral lattice parameters of $a = 2.420(3)$ Å and $\alpha = 109.68(5)°$.

V profile. While the fit to the intense $(1\bar{1}0)_r/(100)_r$ doublet is reasonable, this produces very large misfits to the $(1\bar{1}1)_r$ singlet (as expected by the incorrect d-spacing ratios highlighted in Fig. 5) and greatly underestimates the splittings observed in the higher-angle doublets. Rietveld fits to the profiles collected at higher pressures are equally poor.

However, at pressures immediately above that at which the $(110)_c$ peak splits (36 GPa), the d-spacing ratios *are* displaced by similar amounts about the value of $\sqrt{2}$ (see Fig. 5). Over a small pressure range immediately above the transition, therefore, the rhombohedral model *can* provide a good fit to the diffraction profiles, as demonstrated previously by Jenei *et al.* [7].

It is clear, therefore, that while the diffraction patterns from high-pressure V have the general features expected from a rhombohedral structure in terms of whether individual peaks are split or not, such a structure provides an unacceptably poor fit to the diffraction data. While neither Ding *et al.* nor Takemura showed Rietveld fits to their data, the excellent agreement of their d-spacing ratios with those determined here (Fig. 5) suggests that any Rietveld fits to their data would have been as poor as that shown in Fig. 6.

B. Quasihydrostatic compression of V powder

To determine whether these misfits arose from not using a PTM, we also compressed samples comprising only a small number of grains of V powder within a He PTM, thereby ensuring as hydrostatic a sample environment as possible. These experiments thus reproduce the previous studies of Ding *et al.* and Jenei *et al.* who compressed V powder in He, and in Ar, Ne, and He, respectively [6,7]. The data were
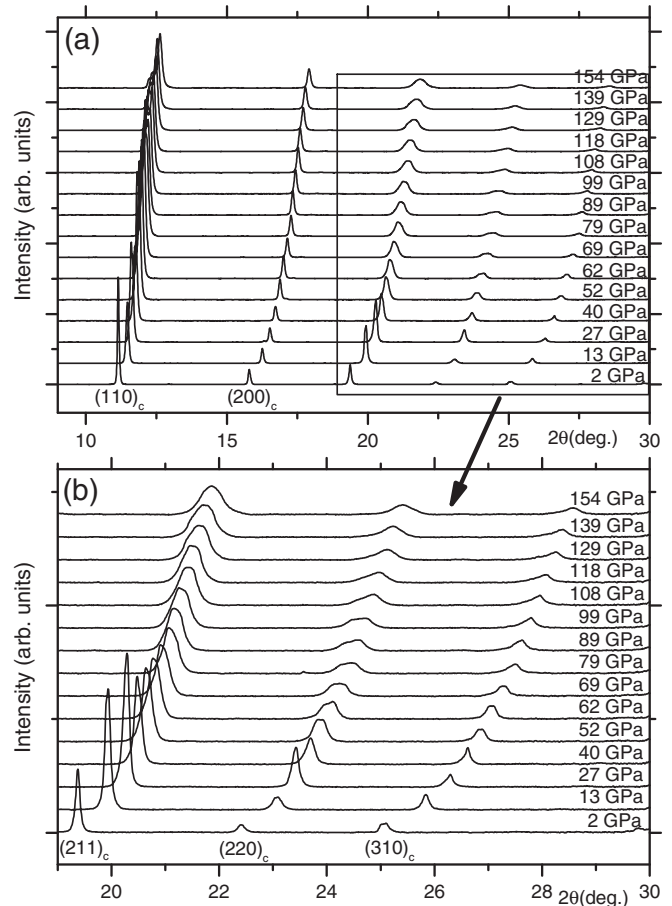

FIG. 7. (a) Diffraction profiles obtained from V powder compressed with a He PTM up to 154 GPa. The incident x-ray wavelength was 0.4119 Å. The peaks in the AP profile are indexed using their bcc indices. (b) Enlarged view of the high-angled region of the profiles. The broadening of the bcc peaks on compression is clear.

again collected at the ESRF in small (2–5 GPa) pressure increments up to 154 GPa. The sample pressure was determined using the ruby fluorescence method, with the sample pressure being measured both before and after each diffraction profile was collected and then averaged. A selection of the collected diffraction profiles in ~10 GPa increments is shown in Fig. 7. Comparison with Fig. 4 reveals similar broad behavior, but the clear splitting of the high-angle peaks observed in the sample loaded without a PTM is not observed in the sample compressed in He.

We again measured the d spacings of the first three Bragg peaks in Fig. 7 and took their ratios, as shown in Fig. 8. The $(110)_c$ peak from the bcc phase was observed to develop an asymmetry just above 10 GPa, some 20 GPa lower than observed in the sample compressed without a PTM, which steadily evolved into a separate peak on further compression. As in the case of the sample compressed without a PTM, the d-spacing ratios clearly do not split symmetrically about the ideal value of $\sqrt{2}$ and so the diffraction profiles will not be fitted by a rhombohedral lattice. Indeed, the d-spacing ratios do not split at all around $\sqrt{2}$, and both ratios are $> \sqrt{2}$ at all pressures. As a result, a Rietveld fit to a diffraction profile
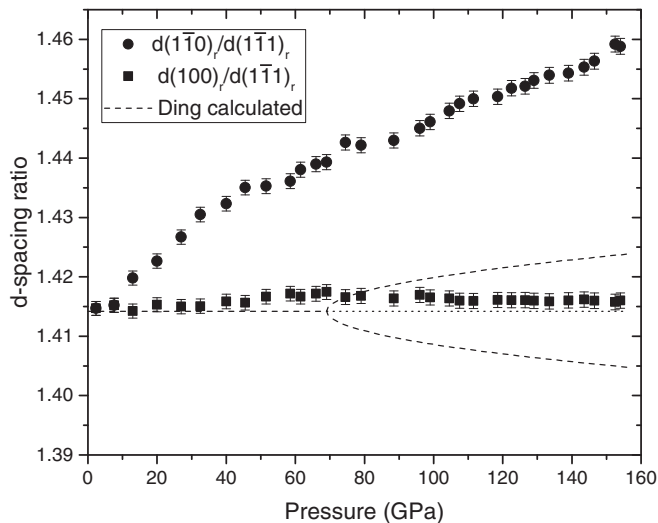
FIG. 8. The pressure dependence of d-spacing ratio of the $(1\bar{1}0)_r$ and $(100)_r$ reflections relative to the $(1\bar{1}1)_r$ reflection for V powder compressed in a He PTM. In the bcc phase the ratio is $\sqrt{2}$, while in the rhombohedral phase the two ratios change such that one is $> \sqrt{2}$ and the other is $< \sqrt{2}$, but their average remains $\sqrt{2}$, as shown by the dashed line. The deviation from this behavior means that a rhombohedral lattice cannot fit the $(1\bar{1}0)_r$, $(100)_r$, and $(1\bar{1}1)_r$ reflections simultaneously. Comparison with Fig. 5 reveals that the deviations from the expected behavior start at lower pressures than in the sample compressed without a PTM, but that the behavior of the $d(1\bar{1}0)_r/d(1\bar{1}1)_r$ ratio is very similar. While the magnitude of the deviation of the $d(100)_r/d(1\bar{1}1)_r$ ratio from $\sqrt{2}$ is similar in both samples, the displacements are in opposite directions.

from the hydrostatic sample at 62 GPa is as poor as that obtained for the nonhydrostatic sample at approximately the same pressure.

Also, the fact that the d-spacing ratios do not split at all around $\sqrt{2}$ also means that unlike in the case of the sample compressed without a PTM, the rhombohedral structure does not provide an adequate fit even immediately above the pressure at which the $(110)_c$ peak splits.

It was clear at this point that the diffraction profiles from neither the nonhydrostatic sample nor the quasihydrostatic one were adequately fitted by a rhombohedral structure, although in both cases the gross changes in the diffraction pattern were consistent with a bcc → rhombohedral transition. It was also clear that where peak positions could be extracted from previously published data, then these data demonstrated exactly the same misfits as observed in the current study.

The reasons for these misfits are not at all clear. One possibility is that the structure of V at high pressure is *not* rhombohedral—despite the almost unanimous agreement of the previous experimental and computational studies that it is. The similarities of the misfits to the expected behavior in a rhombohedral structure are very similar in the nonhydrostatic and quasihydrostatic samples, suggesting that this is the true behavior of V.

Even when using a He PTM, the peak splittings at the bcc → rhombohedral transition are very subtle, and it is difficult to resolve the individual peak positions, even in the high-angle doublets (see Fig. 7). This difficulty arises from an inherent limitation of the powder-diffraction method, that is the overlap of peaks with the same or similar d spacings. Such issues can be overcome using using single-crystal techniques, prompting our final set of studies.

C. Quasihydrostatic compression of [001]-oriented V single crystals

By using single-crystal diffraction techniques, where individual reflections are well separated both spatially on the detector and in the rotation angle of the DAC at which individual reflections satisfy the Bragg condition, we hoped to measure the splitting of the bcc peaks with greater precision than is possible with powder methods, and without interference of other peaks. As we planned to measure only the d spacings of the peaks as a function of pressure, and not their intensity, it was not necessary for the single-crystal to maintain its initial quality to the highest pressures.

The 10-μm-thick V single crystals were grown on a 200 nm thick [001]-oriented single-crystal Mo substrate by Thin Film Laboratory at the University of Aarhus. The presence of the Mo was fortuitous as (i) it allowed us to use the Mo equation of state to determine the sample pressure, and (ii) by collecting and analyzing the reflections from bcc-Mo simultaneously with the peaks from V we were able to monitor any changes to the samples as a result of the nonhydrostatic pressure conditions. A small piece of the V/Mo sample was carefully cut from the larger as-grown sample, taking care to inflict as little damage to the crystal as possible, and placed on one diamond of the DAC. A rotation image was taken before the PTM was added in order to check the quality of the sample. After ensuring the sample quality, the sample chamber was filled with mineral oil and the DAC was carefully closed. Before increasing the pressure further, a full single-crystal data collection was collected in a sequence of contiguous $2°$ oscillations over a total scan range of $\pm 28°$ around the vertical rotation axis ω. The exposure time of 2 s per frame was chosen to ensure that the strongest reflections did not saturate the detector. From these data we were able to obtain an orientation matrix for the sample, and thus assign unique and self-consistent Miller indices to all of the observed Bragg peaks. We used 2 such samples over two visits to the PETRA-III synchrotron to collect quasi-single-crystal data to maximum pressures of 72 GPa, using a wavelength of 0.2898 Å (sample 1) and to 118 GPa, using a wavelength of 0.4850 Å (sample 2).

A rotation image from sample 2 at 8.7 GPa, obtained from a single 2 s exposure during which the DAC was rotated from $\omega = -25°$ to $+25°$, is shown in Fig. 9. As the lattice parameters of V ($a = 3.030$ Å) and Mo ($a = 3.147$ Å) are similar, and the crystallographic alignment of the V and the Mo substrate is the same, then the diffraction image contains pairs of reflections with the higher-angles reflections being from the V. As we planned to collect data from both the bcc and rhombohedral phases of V, and to ensure that consistent indexing was used in both structures throughout, we chose to initially index the rhombohedral phase using the nonprimitive body-centred unit cell where $\alpha' \sim 90°$. We also indexed the Mo reflections using the same indexing, enabling us to compare the behavior of the two materials at each pressure.
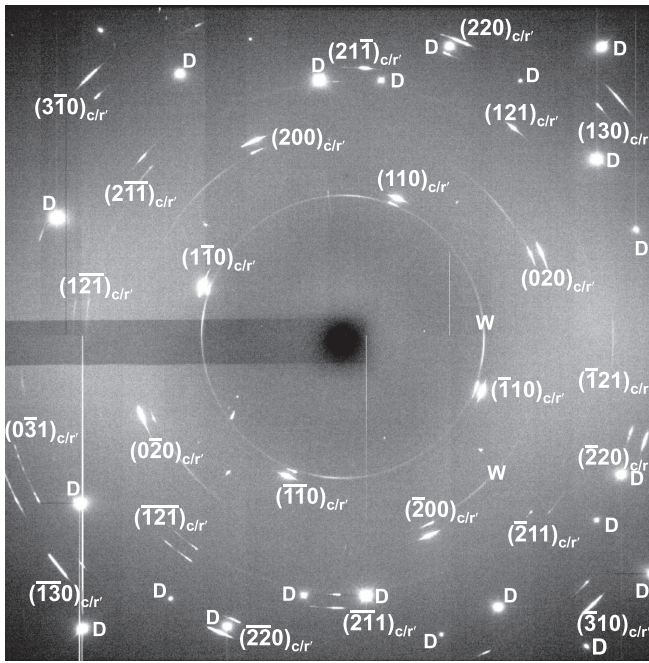
FIG. 9. Rotation ($\pm 25°$ in ω) diffraction image from a V/Mo [001]-oriented single crystal at 8.7 GPa. The most intense reflections from the diamond anvils are identified with "D," while the V/Mo reflections pairs (with the weaker Mo reflections being the lower-angled of the two) are labeled with their bcc Miller indices. To ensure consistency of indexing, the same indices were used to analyze both the cubic and rhombohedral phases, using the nonprimitive body-centred rhombohedral cell to analyze the latter. While the V reflections are elongated azimuthally even at this pressure, their individual d spacings are still measurable precisely without interference from other reflections with the same or similar d spacing. The thin vertical lines on the image are detector artifacts. The two faint Debye-Scherrer rings marked with "W" are from the tungsten gasket.

The lattice parameters were subsequently transformed back to those from the standard primitive unit cell.

Figure 9 demonstrates the power of single-crystal diffraction methods in studying the bcc-rhombohedral transition. The four visible $\{110\}_c$-class reflections should all have the same d spacing in the bcc phase, but after the transition to rhombohedral symmetry, the $(110)_{r'}$ and $(\bar{1}\bar{1}0)_{r'}$ should have the same d spacing (being a Friedel pair), but that d spacing will be different to that of the $(1\bar{1}0)_{r'}/(\bar{1}10)_{r'}$ Friedel pair. The d spacing of each of these four reflections can be measured without interference from the other three, giving a higher-accuracy measurement of the lattice parameters. The same is true for the doublets and triplets evolving from the higher-angled bcc reflections.

Data were collected from sample 1 to 72 GPa in $\sim$3 GPa steps, and from sample 2 to 118 GPa in $\sim$8–10 GPa steps. At each pressure both a rotation image ($\omega = \pm 25°$) and a series of contiguous $2°$ scans (from $-28°$ to $+28°$) were collected. From each data set the d spacings of all visible $\{110\}_{c/r'}$, $\{200\}_{c/r'}$, $\{211\}_{c/r'}$, $\{220\}_{c/r'}$, $\{310\}_{c/r'}$, and $\{400\}_{c/r'}$ classes of reflection from both the V and Mo were measured, and the best-fitting rhombohedral lattice parameters were obtained at each pressure by least-squares fitting
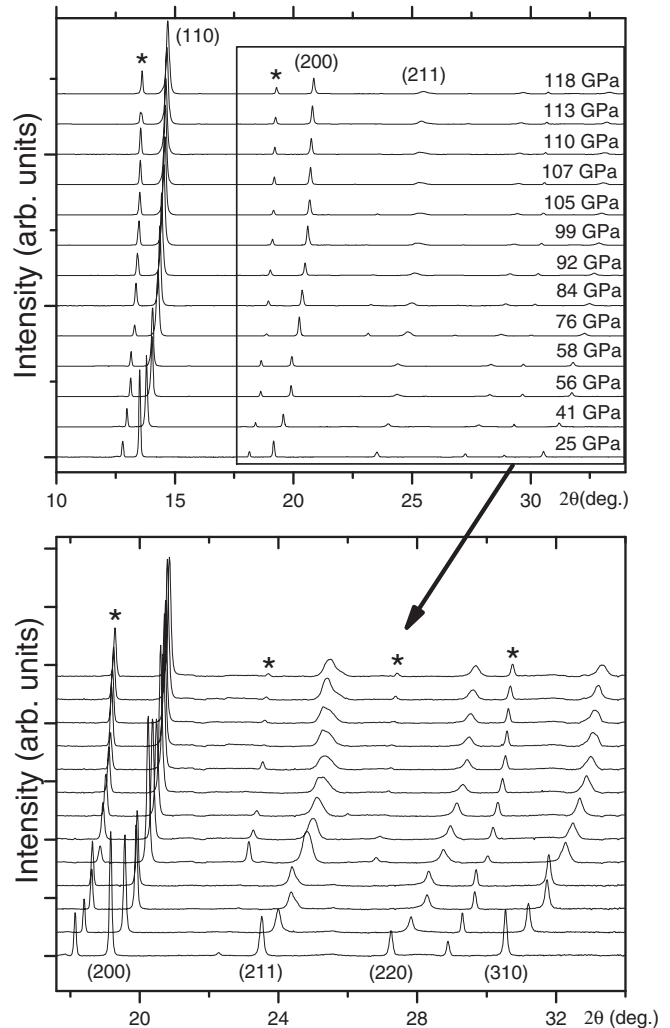

FIG. 10. (a) Pseudo-powder-diffraction profiles obtained by integrating the 2D rotation images obtained from sample 2 of single-crystal V compressed in a mineral oil PTM up to 118 GPa. The peaks from the V are indexed with their cubic Miller indices, while the peaks arising from the Mo substrate are identified with asterisks. (b) Enlarged view of the high-angled region of the profiles.

to the measured d spacings. The number of reflections used in the determination of the lattice parameters was $\sim$30 for sample 1 and $\sim$17 for sample 2 (see Table S1 [24]).

Firstly, for comparison with the data obtained from the powdered samples, we integrated the 2D rotation images obtained from each sample to make pseudo-powder-diffraction profiles, and those obtained from sample 2 are shown in Fig. 10. It is clear that while the peaks broadened slightly with pressure (see also Fig. S1 [24]), somewhat similar to that seen in the quasihydrostatic compression (Fig. 7), the peak splittings seen in the nonhydrostatic compression (Fig. 4) are absent.

However, the different behavior of the single-crystal sample becomes clear when we measure the d spacings of the four visible $\{110\}_{c/r'}$ classes of reflection that make up the first doublet, and, after averaging the d spacings of the Friedel pairs, plot the ratio of each average to that of the (unsplit) second peak, the results of which are shown in Fig. 11. Note
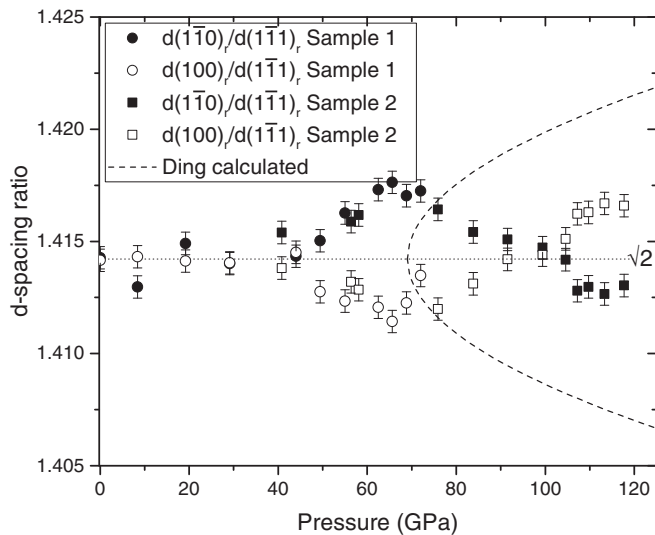
FIG. 11. The pressure dependence of d-spacing ratio of the $(1\bar{1}0)_r$ and $(100)_r$ reflections relative to the $(1\bar{1}1)_r$ reflection (all primitive rhombohedral indexing) for the two samples of single-crystal V compressed in a mineral oil PTM. Note (i) the reduced y-axis scale (0.02 vs 0.06) compared to Figs 5. and 8; (ii) the symmetry of the displacements of the filled/unfilled data points about the ratio of $\sqrt{2}$; and (iii) the fact that the filled/unfilled points cross the $\sqrt{2}$ value at ~100 GPa.

that the y-axis scale of this figure is only ~1/3 of that used in Figs. 5 and 8. It is immediately clear that there are several differences compared to the same plots obtained from the nonhydrostatic/quasihydrostatic powder data. Firstly, the ratios deviate much less from $\sqrt{2}$ in the single-crystal data. Secondly, the two ratios are displaced symmetrically about the 'ideal' value of $\sqrt{2}$. And, thirdly, the ratios cross $y = \sqrt{2}$ at ~100 GPa, suggesting that rhombohedral angle changes from being greater than to less than 109.47° at this pressure (or vice versa, it is not possible to tell from Fig. 11 alone), with the sample being ~cubic at 100 GPa. Such behavior, a transition between two different rhombohedral structures with different deviations from the bcc structure, is very similar to that predicted by previous computational studies [8,10–12,25].

However, in determining the correct pressure dependence of α, that is whether its value refines as > or < 109.47°, depends critically on the initial choice of indexing used to interpret the single-crystal data. The indexing initially determined at ambient pressure for sample 2 is shown in Fig. 9. In the bcc phase, the indexing would be equally valid if the indices were all transformed by a 90° rotation matrix around the crystal normal, such that $(110)_c \rightarrow (\bar{1}10)_c$, $(200)_c \rightarrow (020)_c$, $(301)_c \rightarrow (031)_c$ etc. Using this transformed indexing in the rhombohedral phase results in a different value of α', displaced from 90° in the opposite sense from that of the original indexing, and hence a value of α that is displaced from 109.47° in the opposite sense from that of the original indexing. To check the correct indexing, we fitted each single-crystal data set from both the V and Mo using *both* indexing schemes. At all but two pressures in sample 2, as highlighted in Table S1 in Ref. [24], the better fit to the measured d
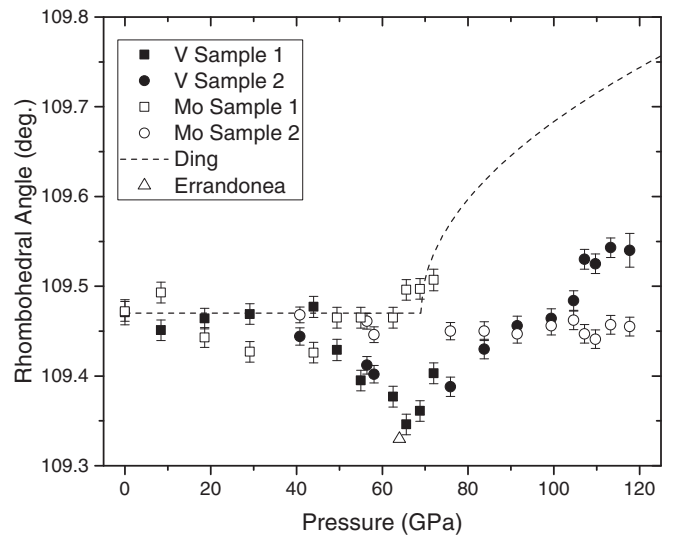

FIG. 12. The rhombohedral angle α in both V and Mo, as determined from the two single-crystal samples. The same indexing was used for both materials. The data from Mo show some scatter about the cubic value of $\alpha = 109.47°$, perhaps arising from the nonhydrostatic pressure environment, but shows no trend away from cubic symmetry. In V, the sample is initially cubic ($\alpha = 109.47°$) until ~40 GPa, above which the angle becomes systematically smaller than the ideal cubic value, reaching a minimum of 109.35(2)° at 66 GPa. On further compression α then increases quasilinearly, passing back through the cubic value at 100 GPa, and increasing to 109.55(2)° at 118 GP, the highest pressure reached with sample 2. The change in α reported by Ding *et al.* [6], and the value determined by Errandonea *et al.* [15] from a Rietveld refinement at 64 GPa, are also shown for comparison.

spacings from the V was obtained with the indexing that gave α' (and hence α) first decreasing from its cubic value with pressure, and then increasing, as shown for α in Fig. 12. The same indexing scheme also gave the better fits to the Mo peak positions at all pressures for sample 2, and at all but two pressures for sample 1, where the fit was only slightly poorer. Despite showing no evidence of any peak splittings in the pseudo-powder diffraction integrated profiles (Figs. 10 and S1), the individual d spacings of the reflections that make up the $(110)_c$ and $(310)_c$ doublets are slightly different (as illustrated in Fig. S2), thereby giving the changes in α shown in Fig. 12.

Also shown in Fig. 12 is the pressure dependence of α reported by Ding *et al.* [6] and the value determined by Errandonea *et al.* [15] from a Rietveld refinement at 64 GPa. It is clear that the value of α determined by Errandonea *et al.* [15] at 64 GPa, the highest pressure at which a Rietveld fit has been reported and the only study in which α has been reported as <109.47°, is in excellent agreement with the current data. However, while the single-crystal data suggest a transition between two different rhombohedral structures, as predicted previously [8,10–12,25], the deviations from cubic symmetry are the reverse of those predicted in these studies, and are very much smaller. This is illustrated in Fig. 13, which shows the angular deviations from 109.47° predicted by Wang *et al.* at 0 K [12]. The rhombohedral angles predicted
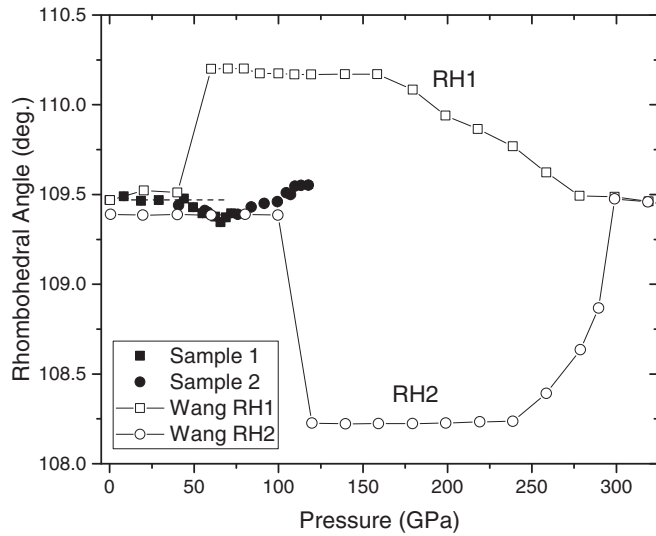
FIG. 13. The rhombohedral angle α as determined from the two single-crystal samples in the current study, compared to that predicted by Wang *et al.* [12] in their two rhombohedral phases, RH1 and RH2, up to 320 GPa. The rhombohedral angles predicted by other computational studies are similar [8,10,11]. The calculated rhombohedral angles (at 0 K) are clearly very much larger than those observed (at 300 K), and the sense of those distortions, that is, whether α is $>$ or $<$ 109.47°, is the reverse of that observed.

by other computational studies are similar [8,10,11]. We also see no volume discontinuities over the full pressure range of our single-crystal studies, as illustrated in Fig. 14, in contrast to the first-order transitions predicted by the computational studies.
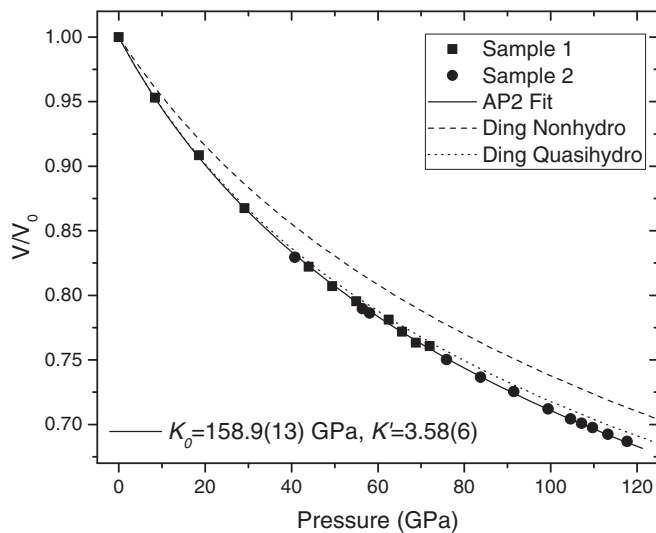

FIG. 14. The compressibility of V to 120 GPa, as determined from the single-crystal data. A fit using an AP2 equation of state [26] is shown, from which the zero pressure bulk modulus K_0 and its pressure derivative K' were determined to be 158.9(13) GPa and 3.58(6), respectively. Also shown are the compressibility curves reported by Ding *et al.* [6] from their nonhydrostatic and quasihydrostatic powder data.

The compressibility of V to 120 GPa, as determined from the single-crystal data, is shown in Fig. 14. A fit to the data using an AP2 equation of state [26] is shown, from which the zero pressure bulk modulus, K_0, and its pressure derivative, K', were determined to be 158.9(13) GPa and 3.58(6), respectively. The zero-pressure volume was fixed at 13.82 Å³ per atom. Also shown for comparison are the compressibility curves determined by Ding *et al.* [6] from their nonhydrostatic and quasihydrostatic powder data.

Our single-crystal data show V to be slightly more compressible than that determined by Ding *et al.* from their quasihydrostatic powder data [6]. While one could also make a comparison with the compressibility obtained from our own quasihydrostatic powder data (Fig. 7), the inability of a rhombohedral structure to fit even the first three peaks of these data, as demonstrated in Fig. 8, would make any agreement little more than fortuitous. We stress that while Ding *et al.*'s nonhydrostatic powder data are completely consistent with our own—and neither fit a rhombohedral structure adequately (Fig. 5)—we cannot determine whether the quasihydrostatic data of Ding *et al.* fit the rhombohedral structure or not, and therefore whether the agreement shown in Fig. 14 is also no more than fortuitous.

VI. DISCUSSION

There is agreement in the literature about the existence of a pressure-induced bcc-rhombohedral transition in V at 30–70 GPa, and the *gross* changes observed in the diffraction patterns from V on compression are indeed consistent with a change in symmetry from cubic to rhombohedral, However, our analysis of the previously published diffraction profiles suggests that in all but one of them a rhombohedral structure provides an inadequate fit to the data. That lone study of Errandonea *et al.* [15] is also the only diffraction study to publish a Rietveld refinement above 30 GPa, well into the rhombohedral phase, and to determine that the rhombohedral angle at that pressure is *smaller* than the cubic value of 109.47°.

Our own powder diffraction data collected without a PTM are completely consistent with these previously published data, and the peak positions are inconsistent with a rhombohedral structure. The same is true for powder diffraction data obtained from vanadium powder compressed quasihydrostatically in a He PTM.

In contrast to the results obtained in our powder studies, the symmetry of the d-spacing ratios about $\sqrt{2}$ illustrated in Fig. 11 shows that these single-crystal data, despite being collected from a sample not compressed in He, *do* fit a rhombohedral lattice at all pressures above 40 GPa, and that the resulting rhombohedral angles are much smaller than previously reported—by either experiment or computation.

We are presently unable to explain the dramatic differences between the results obtained from our single-crystal and powder data, particularly the powder data obtained from samples compressed quasihydrostatically in He. The bcc phase of V is mechanically unstable under trigonal shear, with the instability (softening) of the trigonal shear elastic constant (C_{44}) thought to be primarily due to intra-band nesting of the Fermi surface [5]. The differences in behavior we observe may then

arise from a very high sensitivity of these elastic and electronic effects to the hydrostaticity of the sample environment. If so, then the effects are much larger than those seen in any other elemental metal.

A combination of a material's anisotropic elastic properties, and a nonhydrostatic pressure environment, may result in an (hkl)-dependent displacement of the peaks in a diffraction pattern as a result of the differential strains experienced by the different diffraction planes [27]. It is then possible that the trigonal shear instability in V results in peak displacements that are larger than those typically observed in other materials, resulting in the poor fits to a rhombohedral lattice. Such effects can be investigated and quantified using the so-called radial diffraction geometry, where the axis of the DAC, along which the principal stress is assumed to act, is placed approximately perpendicular to the x-ray beam rather than parallel to it, as was the case in the axial diffraction geometry used in the current experiments [28]. The angle (ψ) between the diffraction plane normals and the principal stress direction then changes with azimuth around each Debye-Scherrer ring, enabling the variation in each peak's position to determined as a function of ψ [28]. In such studies, if a peak position is measured at $\psi = 54.7°$, then lattice strain theory [27] predicts that it is unaffected by the differential strain. The lattice parameters determined from such peak positions will then be equivalent to those determined in a hydrostatic pressure environment, and should fit a lattice.

Fortuitously, such a study has been made by Xiong and Liu of polycrystalline V compressed without a PTM to 70 GPa [18]. In radial diffraction profiles collected at $\psi = 54.7°$, which should be unaffected by differential strains, the relative peak positions should be in excellent agreement with those predicted by the cubic or rhombohedral structure. Surprisingly, this is not the case, as illustrated in Fig. 15 which shows the pressure dependence of the ratio of the center of the $(1\bar{1}0)_r/(100)_r$ doublet relative to that of the $(1\bar{1}1)_r$ peak. This should remain constant at $\sqrt{2}$ in both the cubic and rhombohedral phases, as observed in our single-crystal data but not in our powder data (Fig. 15). Xiong and Liu's data clearly do not show the expected behavior at $\psi = 54.7°$, not even in the bcc phase at 16 GPa. The deviations show that the diffraction profiles still do not fit a cubic or rhombohedral lattice, but also that the deviations from ideal behavior are clearly very different to those observed using a standard axial diffraction geometry. Specifically, the center of the $(1\bar{1}0)_r/(100)_r$ doublet is displaced to higher angles (lower d spacing) than that expected from the position of the $(1\bar{1}1)_r$ peak when using a radial diffraction geometry, while the center of the doublet is located at lower angles when using an axial diffraction geometry.

The behavior of the V at $\psi = 54.7°$ is therefore *not* that expected for a material free from differential strain, and it is clearly very different to that observed in previous standard (axial) diffraction geometry experiments. The modeling used by Xiong and Liu assumes that the principal strain direction lies along the DAC axis and that the strain is cylindrical around that axis. While the axial diffraction geometry used in our experiments means that we cannot determine the 2θ position of each Bragg peak at $\psi = 54.7°$, we can simulate what effect the same cylindrical stress distribution assumed
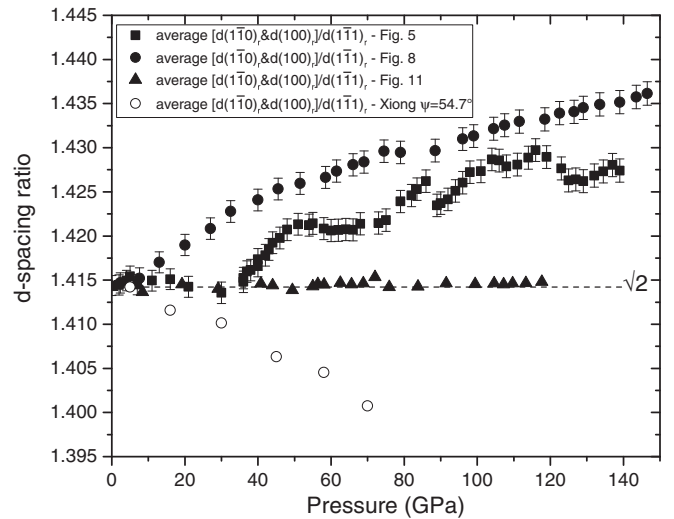

FIG. 15. The d-spacing ratio of the $(1\bar{1}0)_r/(100)_r$ doublet (as determined from its midpoint) relative to that of the $(1\bar{1}1)_r$ peak, as determine from the radial diffraction data reported by Xiong *et al.* at $\psi = 54.7°$ (○). The ratio should remain fixed at $\sqrt{2}$ in both the bcc and rhombohedral phases. Also shown for comparison are the same ratios obtained from our powdered sample compressed without a PTM (■), the powdered sample compressed in a He PTM (●), and from the two single-crystal samples (▲). For the single-crystal data, the error bars are smaller than the symbols used to plot the points and have been omitted.

by Xiong and Liu would have on our diffraction profiles using the methodology described by Higginbotham and McGonegle [29].

Figure 16 shows the effect of changing the strain along the DAC axis (ϵ_{zz}) while keeping the strain perpendicular to this (ϵ_{xx}) constant, such that the differential strain ($\epsilon_{zz} - \epsilon_{xx}$) varies from -5% to $+5\%$, some $10\times$ larger than the differential strain reported by Xiong and Liu [18]. These strains are applied to the calculated diffraction pattern from the best-fitting rhombohedral structure to the data shown in Fig. 6 ($a_r = 2.420$ Å and $\alpha = 109.68°$). The effects of the differential strain are to alter the positions of the Bragg peaks relative to each other, but it is clear that the peak *splittings* are unaffected. Hence, while Lebail fits to these profiles give slightly different values of a_r, ranging from 2.415 Å for profile (a) to 2.426 Å for profile (e), the same value of $\alpha = 109.68°$ is found in all cases. As a result, changing the differential strain, even over this large range, does not increase the splittings of the $(20\bar{2})_r/(200)_r$ and $(21\bar{2})_r/(21\bar{1})_r$ doublets to the extent needed to fit the diffraction data, as highlighted in the inset to Fig. 16.

These simulations and the study of Xiong and Liu have assumed that the differential strain is along the DAC axis, and it is, of course, possible that this was not the case. Indeed, if the gasket hole was expanding, then this might lead to the sample experiencing a reduced stress in one of the transverse directions. In such cases a much more extensive mapping of the peak positions as a function of ψ (the angle between the diffraction plane normals and the principal stress direction) would be needed to determine the exact direction of the latter. A much more detailed radial diffraction study, making no
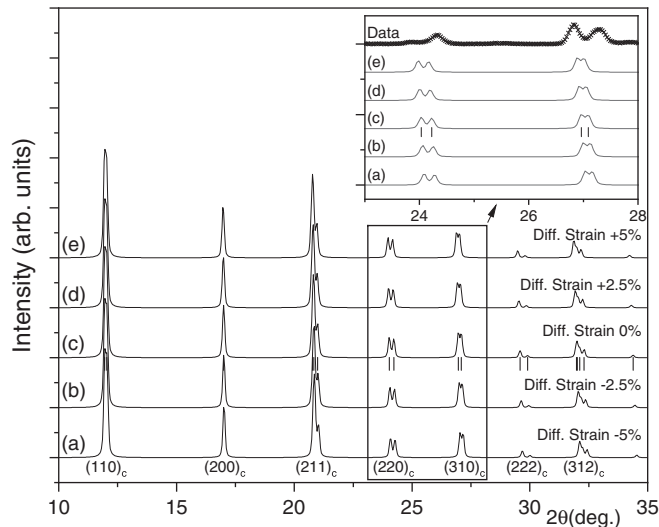
FIG. 16. The calculated diffraction profiles from rhombohedral vanadium with $a = 2.420$ Å, $\alpha = 109.68°$ experiencing differential strains of (a) -5% to (e) $+5\%$. Profile (c) shows the profile unaffected by strain, with the calculated peak positions marked by tickmarks beneath the profile. The effects of the differential strain are to move the positions of the Bragg peaks relative to each other, but the peak *splittings* are unaffected. The inset shows enlarged views of the $(220)_c$ and $(310)_c$ reflections [which split into the $(20\bar{2})_r/(200)_r$ and $(21\bar{2})_r/(21\bar{1})_r$ doublets], and also the observed diffraction data at 61 GPa (the same data shown in Fig. 6). It is clear that the larger peak splittings observed in the data cannot be explained by a differential strain model.

pre-assumptions about the strain distribution, would then be required.

VII. CONCLUSIONS

A series of detailed powder and single-crystal diffraction studies, utilising different pressure transmitting media, reveals that the high-pressure structural behavior of V is not as previously reported. Our nonhydrostatic powder data are completely consistent with that published previously, and cannot be fitted with the rhombohedral structure almost universally agreed to be the stable phase of V above ~ 50 GPa. Our data from V powder compressed in a He PTM show exactly the same issues and also cannot be fitted with a rhombohedral structure. Single-crystal data collected on two samples to 118 GPa *do* fit a rhombohedral lattice above 40 GPa, with the rhombohedral angle α first *decreasing* below the cubic value

of 109.47° to 109.35° at 65 GPa, before then *increasing*, passing back through cubic symmetry at ~ 100 GPa, and reaching a value of 109.54° at 120 GPa. This decrease-then-increase behavior of α is the opposite of that predicted in all previous computational studies, and the measured rhombohedral angles are also very much smaller than predicted.

Finally, given the very small deviations from cubic symmetry measured in the single crystal, we should ask whether the V really does undergo a transition to a rhombohedral structure above 40 GPa. The data collected from the single-crystal of Mo simultaneously with that from V reveal the degree of scatter about $\alpha = 109.47°$ observed even in a cubic structure. The deviations observed in V are ~ 4 times larger than those observed in the Mo, however, and they exhibit a clear pressure dependence not seen in the Mo. The data therefore suggest that there is a cubic-rhombohedral transition in V, but that, at least below 120 GPa, the deviations from cubic symmetry are very small. It would be interesting to repeat the single-crystal experiment in the future using both [011] and, especially, [111]-oriented samples. In the latter case, any preferential stress along the DAC axis would be acting directly along the direction of the rhombohedral distortion, perhaps elastically increasing the rhombohedral angle α. Future experiments are planned.

[1] K. Takemura, in *Proceedings of the International Conference on High Pressure Science and Technology, AIRAPT-17 (Honolulu, July 1999)*, edited by M. Manghnani, W. Nellis, and M. Nicol (Universities Press (India) Ltd., Hyderabad, 2000), pp. 443–444.

[2] Y. Nakamoto, K. Takemura, M. Ishizuka, K. Shimizu, and T. Kikegawa, in *Proceedings of the Joint 20th AIRAPT - 43rd EHPRG Conference on Science and Technology of High Pressure* (Karlsruhe, Germany, 2005).

[3] M. Ishizuka, M. Iketani, and S. Endo, Phys. Rev. B **61**, R3823 (2000).

[4] N. Suzuki and M. Otani, J. Phys.: Condens. Matter **14**, 10869 (2002).

[5] A. Landa, J. Klepeis, P. Söderlind, I. Naumov, O. Velikokhatnyi, L. Vitos, and A. Ruban, J. Phys.: Condens. Matter **18**, 5079 (2006).

[6] Y. Ding, R. Ahuja, J. F. Shu, P. Chow, W. Luo, and H. K. Mao, Phys. Rev. Lett. **98**, 085502 (2007).

[7] Z. Jenei, H. P. Liermann, H. Cynn, J. H. P. Klepeis, B. J. Baer, and W. J. Evans, Phys. Rev. B **83**, 054101 (2011).

[8] B. Lee, R. E. Rudd, J. E. Klepeis, P. Söderlind, and A. Landa, Phys. Rev. B **75**, 180101(R) (2007).

[9] W. Luo, R. Ahuja, Y. Ding, and H.-k. Mao, Proceedings of the National Academy of Sciences **104**, 16428 (2007).

[10] S. L. Qiu and P. M. Marcus, J. Phys.: Condens. Matter **20**, 275218 (2008).

[11] A. K. Verma and P. Modak, Europhys. Lett. **81**, 37003 (2007).

[12] Y. X. Wang, Q. Wu, X. R. Chen, and H. Y. Geng, Scientific Reports **6**, 32419 (2016).

[13] J. H. P. Klepeis, H. Cynn, W. J. Evans, R. E. Rudd, L. H. Yang, H. P. Liermann, and W. Yang, Phys. Rev. B **81**, 134107 (2010).

[14] Y. Yu, Y. Tan, C. Dai, X. Li, Y. Li, Q. Wu, and H. Tan, Appl. Phys. Lett. **105**, 201910 (2020).

[15] D. Errandonea, S. G. MacLeod, L. Burakovsky, D. Santamaria-Perez, J. E. Proctor, H. Cynn, and M. Mezouar, Phys. Rev. B **100**, 094111 (2019).

[16] Y. Zhang, Y. Tan, H. Y. Geng, N. P. Salke, Z. Gao, J. Li, T. Sekine, Q. Wang, E. Greenberg, V. B. Prakapenka, *et al.*, Phys. Rev. B **102**, 214104 (2020).

[17] T. Hahn and H. Klapper, *International Tables for Crystallography, Volume A: Space Group Symmetry*, International Tables for Crystallography (Kluwer, Dordrecht, Boston, London, 2002), 5th ed., https://link.springer.com/referencework/10.1107/97809553602060000100.

[18] L. Xiong and J. Liu, Chin. Phys. B **27**, 036101 (2018).

[19] D. Errandonea (private communication).

[20] T. S. Sokolova, P. I. Dorogokupets, A. M. Dymshits, B. S. Danilov, and K. D. Litasov, Computers & Geosciences **94**, 162 (2016).

[21] C. Prescher and V. B. Prakapenka, High Pres. Res. **35**, 223 (2015).

[22] V. Petricek, M. Dusek, and L. Palatinus, Z. Kristallographie - Crystalline Materials **229**, 345 (2014).

[23] T. J. B. Holland and S. A. T. Redfern, Mineral. Mag. **61**, 65 (1997).

[24] See Supplemental Material at http://link.aps.org/supplemental/10.1103/PhysRevB.103.134103 for additional table of additional crystallographic information and some additional figures.

[25] B. Lee, R. E. Rudd, J. E. Klepeis, and R. Becker, PRB **77**, 134105 (2008).

[26] W. B. Holzapfel, High Pres. Res. **16**, 81 (1998).

[27] A. K. Singh, J. Appl. Phys. **73**, 4278 (1993).

[28] J. Liu, Chinese Phys. B **25**, 076106 (2016).

[29] A. Higginbotham and D. McGonegle, J. Appl. Phys. **115**, 174906 (2014).